Phase diagram of externally modulated Rayleigh-Bénard system near the codimension-two point

Barbara J. A. Zielinska, David Mukamel, and Victor Steinberg
Department of Physics, Weizmann Institute of Science, Rehovot, Israel

Shmuel Fishman
Department of Physics, Technion, Haifa, Israel
(Received 9 June 1986)

The phase diagram of an externally modulated Rayleigh-Bénard system of binary mixtures near the codimension-two (CT) point is analyzed. The amplitude equation associated with this system is considered and the dynamical behavior is obtained by numerical integration of the equations of motion. We find that close to the CT point the system exhibits chaotic behavior, which in some region of the phase diagram *coexists* with the conductive state. It is suggested that these features may be observed experimentally even for small amplitude of the modulation as compared with the critical temperature difference ΔT_c of the unmodulated system.

I. INTRODUCTION

Considerable progress has been made in recent years in understanding phenomena occurring in hydrodynamic systems in the weakly nonlinear regime, where an approximation of just a few modes is very often sufficient. Close to the onset of the convective instability the behavior of the nonlinear system may be described by the equations of motion of just one or a few modes, derivable from the full set of hydrodynamic equations.[1] One of the examples of such a description is the amplitude-equation formalism.[2] This formalism has been extensively used for studying various hydrodynamic systems in confined geometries such as Rayleigh-Bénard or Taylor instabilities. The critical behavior near the threshold predicted for these systems has then been tested experimentally.[3] The amplitude-equation formalism has also been applied to Rayleigh-Bénard systems of binary mixtures.[4] In these systems one finds two kinds of instabilities: stationary and oscillatory.[5] The instability lines intersect at a so-called codimension-two (CT) point.[6–9] As one proceeds into the convective phase, further bifurcations take place leading to a weak-turbulence regime, where several modes strongly interact with each other. However, far from threshold the amplitude equation may no longer be valid. It would be of interest to consider hydrodynamic systems in which the weakly turbulent regime exists sufficiently close to the first convective instability, where the amplitude equation formalism may be applied. It has recently been suggested[10] that Rayleigh-Bénard systems of binary mixtures, in which the temperature gradient is periodically modulated, exhibit chaoitc behavior close to the first instability threshold. To describe the behavior of such a hydrodynamic system close to a CT point with modulated temperature gradient we employ a modified amplitude equation which accounts for the presence of time periodic modulation.[10] Because of its relative simplicity this equation can be readily analyzed for chaotic properties.

Consider a Rayleigh-Bénard system, which consists of a fluid layer between two plates in a vertical temperature gradient ΔT. For small values of ΔT the system is in a steady state characterized by the absence of motion. For sufficiently large ΔT a motion of the fluid sets in and an instability develops. In the case of a simple fluid this instability is stationary and the behavior of the fluid close to the instability threshold may be described by a one-mode Landau-type equation, namely the amplitude equation.[2] In this description it is assumed that close enough to the instability threshold the behavior of the fluid will be dominated by the mode which becomes unstable first. This instability is called stationary since after some equilibration time the velocity at any point in the fluid stays constant. More complicated hydrodynamic systems, such as binary mixtures[11] or viscoelastic fluids,[12] display two kinds of flow patterns: stationary and oscillatory, depending on the values of external parameters. In the case of binary mixtures the external parameters are the gradient of the temperature ΔT and the gradient of the concentration ΔC, while for the viscoelastic fluid they are ΔT and the relaxation time of the stress tensor. In the oscillatory instability the velocity at any point in the fluid changes periodically with some characteristic frequency.

For certain values of the external parameters the stationary and oscillatory bifurcation lines intersect and consequently the two flow patterns intersect at onset. Such an intersection point of two instability lines results in a multicritical point which is of the CT type. Recently extensive theoretical as well as experimental activity was focused on analysis of amplitude equations describing the fluid near a CT point and their phase diagrams.[6–9,13] At the CT bifurcation point two modes become unstable simultaneously. Consequently the amplitude equation describing the behavior of the fluid near such a point is two dimensional. Depending on whether the linear part of this amplitude equation is diagonalizable at the multicriticality, one can distinguish between two kinds of CT points namely those belonging to the $\binom{01}{00}$ Jordan normal form (nondiagonalizable case) or $\binom{00}{00}$ Jordan normal form (diagonalizable case).[14] The binary mixture is an example of a CT point of the first kind[6] while the viscoelastic fluid is an example of a CT point of the second kind.[13] In what follows we concentrate on the CT point of the first kind. We believe, however, that some results of this paper, such as the existence of chaotic trajectories when the temperature gradient is periodically modulated, will also be valid for the CT point of the second kind.

The influence of modulation on the stationary instability in the Rayleight-Bénard convection has recently been studied theoretically and experimentally.[15–19] In the case of pure liquids new nonlinear phenomena occur for modulation amplitudes which are comparable to the critical temperature difference of the unmodulated system.[15–17] Such amplitudes are not easily achievable in experiment. On the other hand, we find that in binary mixtures in the vicinity of the CT point, interesting nonlinear phenomena occur even for small modulation amplitudes as compared to the critical temperature difference. Therefore experimental observation of these phenomena is expected to be much easier.

In the present work we introduce an amplitude equation for periodically modulated Rayleigh-Bénard system of binary mixtures near the CT point. The phase diagram associated with this equation has then been studied by numerical integration of the equations of motion. The numerical analysis shows that, for the model considered, the presence of modulation close to a CT point results in rich variety of new bifurcations and in particular in regions in parameter space of chaotic behavior. This numerical analysis was carried out for a physically realistic range of parameters for binary mixtures. The most striking new feature is the presence of chaotic trajectories in a region of parameter space in which the conductive phase of the unmodulated system is stable. Moreover, we find that in certain regions the conductive phase loses its stability and becomes chaotic via intermittency.

The paper is organized as follows. In Sec. II we derive the amplitude equation for periodically modulated binary mixtures close to the CT point. In Sec. III the phase diagram of this model is analyzed. The linear stability analysis of the conductive phase is presented in Sec. III A. Results of numerical analysis of the nonlinear phenomena are given in Sec. III B.

II. THE AMPLITUDE EQUATION IN THE PRESENCE OF THE MODULATION

A binary mixture of miscible fluids in a porous medium placed between infinite plates is considered. We allow for a periodic modulation of the temperature difference between the lower and the upper plates. In this case the instantaneous Rayleigh number is

$$R(t)=[T^l(t)-T^u(t)]\frac{\beta_1 glK}{\nu\kappa}\equiv R_0+R_1\cos(\omega t)\ , \tag{2.1}$$

where $T^l(t)$ and $T^u(t)$ are the temperatures of the lower and the upper plate respectively, $\beta_1=-\rho^{-1}(\partial\rho/\partial T)_{P,c}$ is the thermal expansion coefficient at constant pressure P and concentration c, while g is the gravitational acceleration, l is the height of the fluid layer, K is the permeability, ν is the kinematic viscosity, and κ is the thermodiffusivity. R_0 is the Rayleigh number in the absence of the modulation, R_1 is the amplitude of the modulation and we assume that $R_1/R_0 \ll 1$. The nonlinear equations describing the deviations from the conductive state are, in dimensionless units,[4]

$$(\gamma\partial_t+1)\Delta w-\Delta_2\theta-\Psi\Delta_2 c=0\ , \tag{2.2a}$$

$$R(t)w+(-\partial_t+\Delta-\mathbf{v}\cdot\nabla)\theta=0\ , \tag{2.2b}$$

$$R(t)w+(\mathscr{L}\Delta-\partial_t-\mathbf{v}\cdot\nabla)c-\mathscr{L}\Delta\theta=0\ . \tag{2.2c}$$

Here w is the z component of the velocity field $\mathbf{v}$, θ is the deviation of the temperature from the conduction profile, and c is the concentration of one component. The parameters in these equations are $\gamma=K\kappa/l^2\epsilon\nu$, K is the permeability, ϵ is the porosity, $\Psi=-k_T\beta_2/T\beta_1$ is the separation ratio, $\beta_2=-\rho^{-1}(\partial\rho/\partial c)_{P,T}$, k_T is the thermodiffusion ratio, $\mathscr{L}=D/\kappa$ is the Lewis number, and D is the diffusion coefficient. The horizontal part of the Laplace operator is $\Delta_2=\partial_x^2+\partial_y^2$. In the above equations time is scaled with l^2/κ, velocity with κ/l, temperature with $\nu\kappa/\beta_1 glK$, and concentration with $-\nu\kappa k_T/T\beta_1 gKl$. We assume that the fluid is contained in a rectangular box with sides L_x, L_y, and $l=1$. The boundary conditions for the velocity field $\mathbf{v}=(u,v,w)$, temperature and concentration are taken to be[11]

$$\begin{aligned} &u=0 \quad \text{at } x=0 \text{ and } x=L_x\ ,\\ &v=0 \quad \text{at } y=0 \text{ and } y=L_y\ ,\\ &w=0 \quad \text{at } z=0 \text{ and } z=1\ , \end{aligned} \tag{2.3a}$$

and

$$\begin{aligned} &\partial_x\theta=\partial_x c=0 \quad \text{at } x=0 \text{ and } x=L_x\ ,\\ &\partial_y\theta=\partial_y c=0 \quad \text{at } y=0 \text{ and } x=L_y\ ,\\ &\theta=c=0 \quad \text{at } z=0 \text{ and } z=1\ . \end{aligned} \tag{2.3b}$$

These highly idealized boundary conditions are expected to result in qualitatively similar features to those obtained from physically more realistic rigid boundary conditions for velocity and "no-mass-flux" boundary condition for the concentration field.

Let us first review the results of the linear analysis of Eqs. (2.2) in the absence of modulation, namely for $R_1=0$.[6] Consider a perturbation of the form

$$\begin{bmatrix}\omega(x,z,t)\\ \theta(x,z,t)\\ c(x,z,t)\end{bmatrix}=\begin{bmatrix}w_1\\ \theta_1\\ c_1\end{bmatrix}e^{\sigma t}\cos(\pi x)\sin(\pi z)\ , \tag{2.4}$$

where the critical wave vector in the horizontal direction is taken to be π. Inserting (2.4) in Eqs. (2.2) one finds stationary instability ($\sigma=0$) with the critical Rayleigh number

$$R_{cs}=\frac{4\pi^2\mathscr{L}}{\Psi+\Psi\mathscr{L}+\mathscr{L}}\ , \tag{2.5}$$

and the oscillatory instability ($\sigma=i\omega_0$) with the critical Rayleigh number

$$R_{co}=4\pi^2\frac{1+\mathscr{L}}{1+\Psi}\ . \tag{2.6}$$

The frequency at the onset of the instability is

$$\omega_0^2=-\frac{4\pi^4\mathscr{L}^2}{1+\Psi}(1+\Psi+\Psi\mathscr{L}^{-1}+\Psi\mathscr{L}^{-2})\ . \tag{2.7}$$

The multicritical point is defined by $R_{\rm CT}=R_{co}=R_{cs}$, implying

$$R_{\rm CT}=4\pi^2(1+\mathscr{L}+\mathscr{L}^2)\ . \tag{2.8a}$$

Since $\omega_{\rm CT}=0$, Eq. (2.7) yields

$$\Psi_{\rm CT}=-\frac{\mathscr{L}^2}{1+\mathscr{L}+\mathscr{L}^2}\ . \tag{2.8b}$$

This is an example of a codimension-two point of the first kind (nondiagonalizable case).[6] For $\Psi>\Psi_{\rm CT}$ the first instability is expected to be stationary and for $\Psi<\Psi_{\rm CT}$ it is expected to be oscillatory.

The linear analysis in the presence of a periodic modulation of the temperature gradient is slightly more complicated. We assume that the amplitude of the modulation is small, namely $R_1/R_0\ll 1$, and derive the amplitude equation to lowest order in R_1. We expect the correction to the horizontal critical wave vector to be of $O(R_1^2)$. These corrections may therefore be neglected in the present analysis. Consequently we insert the ansatz

$$\begin{bmatrix} w(x,z,t) \\ \theta(x,z,t) \\ c(x,z,t) \end{bmatrix}=\begin{bmatrix} W(t) \\ \Theta(t) \\ C(t) \end{bmatrix}\cos(\pi x)\sin(\pi z) \tag{2.9}$$

in the linear part of Eqs. (2.2). Taking twice the time derivative of Eq. (2.2a) using Eqs. (2.2b) and (2.2c) one finds

$$2\pi^2\gamma\dddot{W}(t)+2\pi^2[1+2\pi^2\gamma(\mathscr{L}+1)]\ddot{W}(t)-[\pi^2R(t)(1+\Psi)-4\pi^4(\mathscr{L}+1+2\pi^2\mathscr{L}\gamma)]\dot{W}(t)$$
$$-2\pi^4\left[R(t)(\Psi\mathscr{L}+\mathscr{L}+\Psi)-4\pi^2\mathscr{L}+\frac{1}{2\pi^2}(1+\Psi)\dot{R}(t)\right]W(t)=0\ . \tag{2.10}$$

For typical porous medium the parameter γ is small, and may be neglected. Consequently W satisfies

$$\ddot{W}(t)-[a+\epsilon_1\cos(\omega t)]\dot{W}(t)-[b+\epsilon_2\cos(\omega t+\phi)]W(t)=0\ , \tag{2.11}$$

where

$$a=2\pi^2(\mathscr{L}+1)[(R-R_{co})/R_{co}]\ ,$$
$$\epsilon_1=\tfrac{1}{2}(1+\Psi)R_1,\ b=4\pi^4\mathscr{L}[(R-R_{cs})/R_{cs}]\ ,$$
$$\epsilon_2=\tfrac{1}{2}R_1[4\pi^4(\psi\mathscr{L}+\mathscr{L}+\psi)^2+\omega^2(\psi+1)^2]^{1/2}$$

and

$$\tan\phi=\frac{(1+\Psi)\omega}{2\pi^2(\Psi\mathscr{L}+\mathscr{L}+\Psi)}\ .$$

The nonlinear part of the amplitude equation has previously been derived for the unmodulated case.[6] In this derivation one obtains the nonlinear terms at the multicritical point $a=b=0$. Since the coefficients of the nonlinear terms are $O(1)$, their a and b dependence may be neglected for small a and b. The nonlinear terms may also depend on the modulating amplitude R_1. Since R_1 is assumed to be small one may neglect the dependence of the nonlinear terms on R_1 for similar reasons. We therefore consider the following nonlinear amplitude equation:[10]

$$\ddot{W}=[a+\epsilon_1\cos(\omega t)]\dot{W}+[b+\epsilon_2\cos(\omega t+\phi)]W+f_1W^3+f_2W^2\dot{W}\ . \tag{2.12}$$

For binary mixture in a porous medium[6] $f_1=\pi^2/4$ and $f_2=-\frac{1}{4}(\mathscr{L}^{-1}+1)$.

III. PHASE DIAGRAM

A. Linear stability analysis

The phase diagram of an unmodulated Rayleigh-Bénard system of binary mixtures has previously been analyzed.[6] Within the amplitude equation approach this system may be described by the model

$$\ddot{x}=[a+\epsilon_1\cos(\omega t)]\dot{x}+[b+\epsilon_2\cos(\omega t+\phi)]x+f_1x^3+f_2x^2\dot{x} \tag{3.1}$$

with $\epsilon_1=\epsilon_2=0$. Taking $f_2<0$ and $f_1>0$ as expected for binary mixtures, one finds that the phase diagram is given by Fig. 1. In this case there are two transition lines associated with the instabilities of the convective phase: a second-order (forward bifurcation) line I_o leading to an oscillatory phase, and a first-order (inverse bifurcation) line I_s leading to a stationary phase. The two phases are separated by line I_n,[20] on which a heteroclinic connection occurs. The frequency of oscillation vanishes when this line is approached from the oscillatory phase. The phase diagram of the model (3.1) with $R_1\neq 0$ is expected to be rather complicated. In this case the model is equivalent to

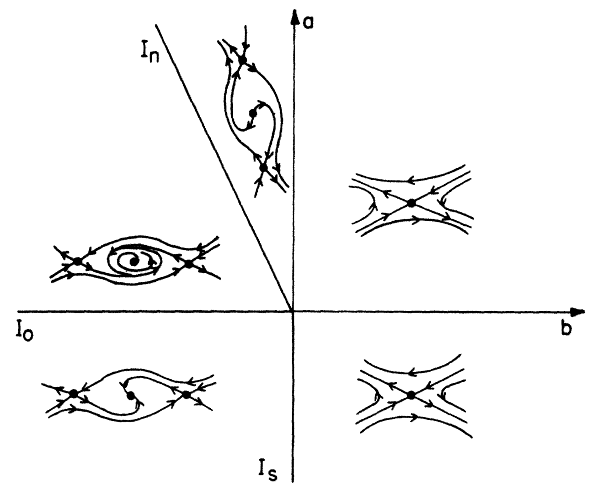

FIG. 1. Phase diagram of Eq. (2.1) for $f_1>0$, $f_2<0$, and $\epsilon_1=\epsilon_2=0$. I_0 is a second-order line separating the conductive phase from the oscillatory one. I_s is a first-order line separating the conductive and the stationary phases. The oscillatory and stationary phases are separated by a nonlinear second-order line I_n. As this line is approached from the oscillatory phase, the frequency of the periodic motion goes to zero.

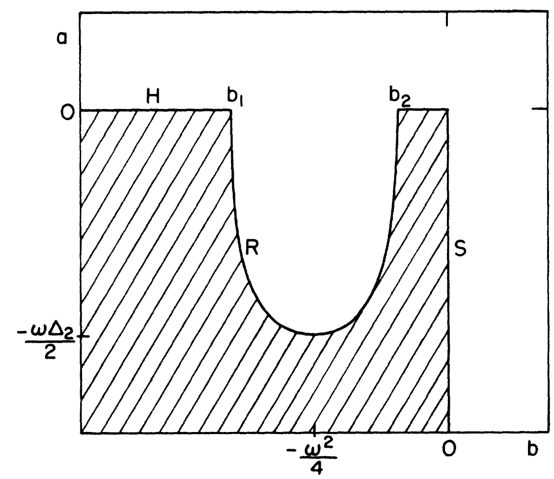

FIG. 2. Stability limits of the conductive phase for small Δ_1 and Δ_2 following from the stability analysis of Eq. (2.2) for fixed Δ_1, Δ_2, and ω. The shaded area corresponds to the stability region of the conductive phase. Along the line S the relevant eigenvalue is zero, while along lines H and R the relevant eigenvalue is purely imaginary. Along R (the resonance tongue) the frequency at the onset is locked to $\omega/2$, where ω is the modulating frequency.

an autonomous map with three variables: x, $\dot{x}$, and t, and therefore it may (and in fact it does) exhibit chaotic trajectories.[21] These trajectories introduce drastic changes in the phase diagram. In this section we consider the phase diagram of the model (3.1) with small nonzero R_1. We first apply linear stability analysis to study the instability lines associated with the conductive phase $x=0$. The results of this analysis are summarized in Fig. 2. We also determine the region in the $a-b$ plane in which heteroclinic orbits exist, when modulation is present. Details of this calculation are given in the Appendix. In Sec. III B we apply numerical methods to study some of the nonlinear features of this phase diagram. However, since the phase diagram is very complicated, this analysis is restricted only to a small region of the parameter space close to the CT point.

Consider now the stability of the $x=0$ conductive phase for small $\Delta_1\equiv\epsilon_1/a$, $\Delta_2\equiv\epsilon_2/b$, and $\phi=0$. The linear part of Eq. (3.1) is then given by

$$\ddot{x}=a[1+\Delta_1\cos(\omega t)]\dot{x}+b[1+\Delta_2\cos(\omega t)]x\ . \qquad (3.2)$$

Using Floquet theorem, we consider a solution of Eq. (3.2) of the form

$$x=e^f \ \text{ with } f=\lambda t+F(\omega t)\ , \qquad (3.3)$$

where $F(\omega t)$ is a periodic function with period 2π. Expanding $F(\omega t)$ in the small parameters Δ_1 and Δ_2 we find

$$f=\lambda t+A\cos(\omega t+\varphi)+O(\Delta_1^2,\Delta_2^2)\ , \qquad (3.4)$$

where A is assumed to be $O(\Delta_1,\Delta_2)$. Inserting (3.3) with (3.4) into (3.2) and keeping terms of order Δ_1 and Δ_2 we find the following expressions for φ, A, and λ:

$$\tan\varphi=\frac{2\lambda-a}{\omega}\ , \qquad (3.5a)$$

$$A=-\frac{\lambda a\Delta_1+b\Delta_2}{[\omega^2+(2\lambda-a)^2]^{3/2}}\ , \qquad (3.5b)$$

$$4\lambda^4-8a\lambda^3+\lambda^2[\omega^2+a^2(5-\tfrac{1}{2}\Delta_1^2)-4b]-\lambda a[\omega^2+a^2(1-\tfrac{1}{2}\Delta_1^2)-4b]-b(\omega^2+a^2)+\tfrac{1}{2}b\Delta_2(b\Delta_2+a^2\Delta_1)=0\ . \qquad (3.5c)$$

The conductive phase is stable as long as $\mathrm{Re}\lambda_i<0$, $i=1,\ldots,4$, where λ_i are the four roots of Eq. (3.5c). An instability takes place when one of the eigenvalues λ_i satisfies $\mathrm{Re}\lambda_{i_0}=0$ while $\mathrm{Re}\lambda_i<0$, $i\neq i_0$. Therefore at threshold λ_{i_0} may either be zero or purely imaginary. Consider first the possibility $\lambda_{i_0}=0$. In this case Eq. (3.5c) takes the form

$$\lambda(\lambda+\alpha)(\lambda^2+\beta\lambda+\gamma)=0 \ \text{ with } \alpha,\beta,\gamma>0\ . \qquad (3.6)$$

Comparing Eq. (3.5) with Eq. (3.6) we conclude that $b=0$ stays the instability surface as long as Δ_1 and Δ_2 are sufficiently small so that the higher-order corrections are negligible. The case of purely imaginary λ is more complicated. In particular if the modulating frequency ω and the frequency of the oscillatory phase Ω are related via $n\omega=2\Omega$ where n is an integer, one expects resonance effects to take place. The nth-order resonance is obtained by considering perturbation expansion to order Δ_1^n,Δ_2^n. Here we restrict ourselves to leading nontrivial order in Δ_1 and Δ_2. The only resonance frequency which can be obtained to this order is $\omega=2\Omega$. We will consider this effect later in this section.

When the resonance condition is not satisfied the stability surface in the case of imaginary λ is determined by the solutions of Eq. (3.5c). It is easy to see that the line $a=0$ is an instability line even for $\Delta_1,\Delta_2\neq 0$, provided b is large and negative. In order to verify that this indeed is the case note that for $a=0$ Eq. (3.5c) becomes

$$\lambda^4+\tfrac{1}{4}\lambda^2(\omega^2-4b)-\tfrac{1}{4}b(\omega^2-\tfrac{1}{2}b\Delta_2^2)=0\ . \tag{3.7}$$

The line $a=0$ is an instability line provided Eq. (3.7) has only negative solutions for λ^2. This is the case for $b\leq\tilde{b}\equiv-\omega^2/4(1+\Delta_2/\sqrt{2})$. One should note that the expansion (3.3) is valid as long as the amplitude A is small, namely $O(\Delta_1,\Delta_2)$. This restriction is satisfied provided $\omega^2+(2\lambda-a)^2$ is $O(1)$ [see Eq. (3.5b)]. For $b=\tilde{b}$ one finds that $\omega^2+(2\lambda-a)^2\simeq O(\Delta_2)\ll 1$. This leads to $A=O(1/\sqrt{\Delta_2})$, indicating that the expansion (3.3), and hence (3.7) are not valid at this point. In fact one can easily verify that Eq. (3.7) is valid for $b\ll\tilde{b}$. The divergence of A for $b\simeq\tilde{b}$ is a manifestation of resonance effects which take place in the vicinity of $\tilde{b}$. For $b\ll\tilde{b}$, and hence for $|b|\gg\omega^2$, the frequency $\Omega=-i\lambda$ at the threshold can be calculated from Eq. (3.7). The result $\Omega\simeq\sqrt{-b}$ is similar to the one found for the unmodulated case.

In order to calculate the instability line near $b=\tilde{b}$ we consider the transition with the resonance frequency $\Omega=\omega/2$. In general the solution of Eq. (3.2) in the case of resonance has the form

$$x(t)=e^{\lambda t}(Be^{i\Omega t}+B^*e^{-i\Omega t})\ , \tag{3.8}$$

where λ is assumed to be real. Equation (3.8) together with Eq. (3.2) yield a polynomial in λ:

$$\lambda^4-2a\lambda^3+\lambda^2\left[2\left[\frac{\omega^2}{4}-b\right]+a^2(1-\tfrac{1}{4}\Delta_1^2)\right]-\lambda a\left[2\left[\frac{\omega^2}{4}-b\right]+b\Delta_1\Delta_2\right]+\left[b+\frac{\omega^2}{4}\right]^2-\tfrac{1}{4}\Delta_2^2b^2+\tfrac{1}{4}a^2\omega^2(1-\tfrac{1}{4}\Delta_1^2)=0\ . \tag{3.9}$$

The stability boundary occurs at $\lambda=0$. This yields the following expression for the resonance curve:

$$a^2(1-\tfrac{1}{4}\Delta_1^2)=\frac{4}{\omega^2}[\tfrac{1}{4}b^2\Delta_2^2-(\tfrac{1}{4}\omega^2+b)^2]\ . \tag{3.10}$$

In what follows we refer to this curve as a resonance tongue. A typical resonance tongue is shown in Fig. 2, where the stability boundaries of the conductive phase resulting from the linear analysis presented in this section are shown. This curve intersects the $a=0$ axis at

$$b=b_1\equiv-\frac{\omega^2}{4}(1+\tfrac{1}{2}\Delta_2)$$

and

$$b=b_2\equiv-\frac{\omega^2}{4}(1-\tfrac{1}{2}\Delta_2)\ .$$

Outside the resonance tongue all the coefficients in the polynomial (3.9) are positive, implying that all solutions for λ are negative. Consequently this is the region of stable conductive ($x=0$) phase. Inside the resonance tongue the free term in polynomial (3.9) is negative, yielding a positive solution for λ. Thus the conductive phase loses its stability along the edge of the resonance tongue and is unstable inside the tongue. For higher resonances, i.e., for $n\omega=\pm 2\Omega$, similar resonance tongues may be calculated. These higher resonances show up in higher order in Δ_1 and Δ_2.

In order to complete the linear stability analysis of the conductive phase we consider the intermediate values of b, namely for $b\lesssim b_1$ and $b\gtrsim b_2$ (see Fig. 2). In these regions one expects the frequency Ω at threshold to deviate considerably from $\sqrt{-b}$ (the value for large negative values of b) and approach continuously the locked frequency $\omega/2$ as b approaches b_1 and b_2. For this purpose we assume that $\Omega\simeq\omega-\Omega$, and consider $x(t)$ of the form

$$x(t)=e^{\lambda t}(Be^{i\Omega t}+Ce^{i(\omega-\Omega)t}+\text{c.c.})\ , \tag{3.11}$$

where the two almost degenerate frequencies Ω and $\omega-\Omega$ have been included. Higher harmonics of ω and Ω may also contribute to $x(t)$, however, they are of higher order in Δ_1 and Δ_2 and may be neglected. In Eq. (3.11) λ is taken to be real. Inserting Eq. (3.11) into Eq. (3.2) one finds the following solvability conditions

$$\lambda^4-2a\lambda^3-\lambda^2[2b+2\Omega(\Omega-\omega)+(2\Omega-\omega)^2-a^2(1-\tfrac{1}{4}\Delta_1)]+\lambda a[2b(1-\tfrac{1}{4}\Delta_1\Delta_2)+2\Omega(\Omega-\omega)+(2\Omega-\omega)^2]+b^2(1-\tfrac{1}{4}\Delta_2^2)+b[\Omega^2+(\Omega-\omega)^2]+\Omega^2(\Omega-\omega)^2-a^2\Omega(\Omega-\omega)(1-\tfrac{1}{4}\Delta_1^2)=0\ , \tag{3.12a}$$

and

$$\{2\lambda^3-3a\lambda^2+\lambda[a^2(1-\tfrac{1}{4}\Delta_1^2)-2b-\Omega(\Omega-\omega)]+\tfrac{1}{2}a[\Omega(\Omega-\omega)+2b-\tfrac{1}{2}ab\Delta_1\Delta_2]\}(2\Omega-\omega)=0\ . \qquad (3.12\text{b})$$

The two equations yield expressions for the critical line and the critical frequency Ω. For $\lambda=0$, Eq. (3.12b) is solved by either $a=0$ or

$$\Omega(\Omega-\omega)+2b-\tfrac{1}{2}ab\Delta_1\Delta_2=0\ .$$

The second possibility is not physical since it leads to negative values of a^2, when inserted into Eq. (3.12a). Consequently the critical line is given by $a=0$, even in the intermediate regime $b\lesssim b_1$, $0>b\gtrsim b_2$. The critical frequency Ω is given by Eq. (3.12a) with $a=\lambda=0$. It can be easily seen, that Ω approaches the resonance frequency $\omega/2$ for b approaching b_1 from below and b_2 from above. For negative values of a all the coefficients in the polynomial (3.12b) are positive, which as previously ensures only negative solution for λ. This means that if the resonance condition is not satisfied the conductive $x=0$ phase is stable in the region of negative a. Conversely for positive a the free term in polynomial (3.12b) is negative, which allows for positive solution for λ.

The results of this section are presented in Fig. 2. This figure corresponds to a cut in parameter space for constant Δ_1, Δ_2, and ω. Only the tongue resulting from the first resonance (i.e., for $\omega=2\Omega$) is shown in this figure. In principle there exist infinitely many smaller resonance tongues corresponding to rational values of Ω/ω. They are not shown in Fig. 2 since the analysis presented in this section is restricted to the lowest nontrivial order in Δ_1 and Δ_2. The shaded area represents the region in which the conductive phase is stable. This phase becomes unstable along the three lines denoted by S, H, and R in Fig. 2. Along S the relevant eigenvalue does not have an imaginary part, as is the case of a stationary instability in the absence of modulation. Here, however, the phase on the right-hand side of the line S can not be stationary, since nonzero Δ_2 does not allow for fixed point solutions. Along H and R the relevant eigenvalue is purely imaginary. The frequency Ω at the onset of the instability varies continuously along the line H and is locked to $\omega/2$ along R.

Consider now the line I_n in Fig. 1. In the unmodulated case one finds heteroclinic orbit along this line. However as one introduces modulation, one expects heteroclinic orbits to exist in a finite region in the a-b plane. The boundaries of this region may be calculated by the Melnikov method.[14] In the Appendix we apply this method to the case $\Delta_1\neq0$, $\Delta_2=0$ and find the two lines I_n^1 and I_n^2 in the a-b plane which bound this region.

B. Numerical results

In this section we report the results of numerical studies of some nonlinear features of modulated Rayleigh-Bénard system of binary mixture. Within the amplitude equation formalism this system may be described by model (3.1) with $f_1>0$ and $f_2<0$. In this case one has to add higher order terms to Eq. (3.1) to ensure stability. We therefore consider the model

$$\ddot{x}=[a+\epsilon_1\cos(\omega t)]\dot{x}+[b+\epsilon_2\cos(\omega t+\phi)]x+f_1x^3+f_2\dot{x}x^2+f_3x^5\ , \qquad (3.13)$$

where a fifth-order term f_3x^5, $f_3<0$, is added. In the unmodulated system Eq. (3.13) yields two stable fixed points. These fixed points coexist in some part of the parameter space (in particular in the neighborhood of line I_n in Fig. 1) with a stable limit cycle. If the distance between these fixed points and the limit cycle in the phase space is small enough the presence of the modulation may result in a "merging" of their respective regions of attraction. This in turn may result in chaotic behavior, where a single trajectory wanders randomly between the remnants of the basins of attraction of the stable fixed points and the limit cycle of the unmodulated system. These interesting phenomena will occur if the coefficient of the fifth-order term will be large enough compared to other coefficients in Eq. (3.13) in order to bring the fixed points and the limit cycle of the unmodulated system sufficiently close to each other. Later in this section we will discuss the physically relevant values of the coefficient f_3 and compare it with other coefficients of Eq. (3.13).

The number of parameters in our model is 9. Scanning this nine-dimensional space is a formidable task. We therefore restrict ourselves to the case in which the parameters ϵ_1, ϵ_2, f_1, f_2, f_3, ω, and ϕ are fixed at physically accessible values and consider the two-dimensional phase diagram in the a-b plane. Moreover, since this study is carried out by performing numerical integration of Eq. (3.13) one is not guaranteed, that one will grasp *all* the important features of the phase diagram, even in this limited range of the parameter space. We hope, however, that in the analysis presented below the gross features of the phase diagram have been elucidated.

Two physical systems have been studied recently, in which the effects of modulation described in this work could be observed. These are the ^{3}He-^{4}He mixtures at low temperatures,[22] and binary mixtures of, say, ethanol and water at room temperatures.[23] In both cases the experimentally controlled parameters are the temperature gradient ΔT, the concentration gradient ΔC across the fluid layer, the amplitude R_1 and the frequency ω of the modulation. By varying ΔT and ΔC one controls the changes in the Rayleigh number R_0 [see Eq. (2.1)]. The Lewis number $\mathscr{L}=D/\kappa$ and the separation ratio $\Psi=-k_T\beta_2/T\beta_1$ [see Eq. (2.2)] are determined by the mean temperature and concentration. Ψ changes from negative to positive values very close to the CT point and is very small in the region relevant to the phenomena that are studied in the present work. In the ^{3}He-^{4}He experiment Ψ is of the order of 10^{-4} and in the room-temperature experiment it is of the order of 10^{-3}–10^{-4}. On the other hand the Lewis number $\mathcal{L}$ changes only slightly across the relevant region of ΔT and ΔC. Typically it values range from $\mathcal{L} \approx 4\times 10^{-2}$ in the helium experiment to $\mathcal{L} \approx 10^{-2}$ in the room-temperature experiment. The coefficient f_3 was recently calculated for the binary mixture in porous medium.[24] Applying this result to the ^{3}He-^{4}He and the water-ethanol mixture one finds that the ratio f_3/f_1 varies considerably with $\mathcal{L}$ and Ψ, typically from below unity to over a hundred. In the numerical results presented below we take $f_1=1$, $f_2=-1$, and $f_3=-7$. The integration of the equation of motion for different values of f_3 shows that the qualitative features of the phase diagram are unchanged as long as the ratios $|f_3|/f_1$ and f_3/f_2 are not below unity.

We have performed numerical integration of Eq. (3.13) for two choices of ϵ_1, ϵ_2, ω, and ϕ corresponding to the ^{3}He-^{4}He mixture and to the ethanol-water mixture, respectively. Since the interesting phenomena take place for ϵ_1 and ϵ_2 comparable to or larger than a and b (or for $\Delta_1,\Delta_2 \geq 1$), they lay in a region of the parameter space far from the domain of validity of the expansions presented in Sec. II A. For large Δ_1 and Δ_2 higher-order corrections are not negligable, and therefore the stability lines presented in Fig. 3, and in particular the shape of stability tongue differ from these of Fig. 2. In the following analysis of Eq. (3.13) the stability boundaries of all phases are determined numerically.

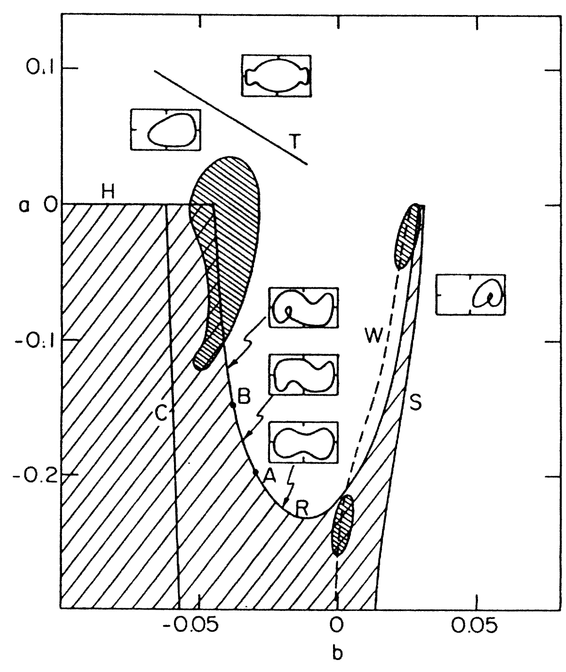

FIG. 3. The phase diagram of Eq. (2.13) for $f_1=1$, $f_2=-1$, $f_3=-7$, $\epsilon_1=0.009$, $\epsilon_2=0.08$, $\omega=0.273$, and $\phi=0$. The shaded area is the stability region of the conductive phase. The heavily shaded areas denote approximately the regions of chaotic trajectories. The insets show schematic trajectories in the corresponding regions (for details see text).

First we choose $\epsilon_1=0.09$, $\epsilon_2=0.08$, and $\omega=0.273$. At resonance (i.e., $\Omega=\sqrt{-b}=\omega/2$) these modulation parameters correspond to the values of the Lewis number $\mathcal{L}=4.3\times 10^{-2}$ and the separation ratio $\Psi=-0.48\times 10^{-5}$ which are realistic values for ^{3}He-^{4}He mixtures. The corresponding amplitude of the modulation is $R_1=0.18$, which gives a ratio $R_1/R_0 \simeq 0.005$ ($R_0=4\pi^2$ in dimensionless units). Our numerical studies show that such a small amplitude of the modulation already yields interesting nonlinear behavior. This is contrary to the case of pure fluids,[15–17] where modulation driven bifurcations occur only for R_1/R_0 of $O(1)$. The above values of Ψ and $\mathcal{L}$ imply a small phase $\phi=18°$ as defined in Eq. (2.11). We have checked several other values of ϕ and concluded, that small ϕ does not change the qualitative results. Therefore in the phase diagram described below the phase ϕ was taken equal to zero.

The phase diagram of Eq. (3.13) for the above chosen values of ϵ_1, ϵ_2, ω, and ϕ is shown in Fig. 3. The shaded area corresponds to the region in which the conductive phase is stable. The boundary of this phase consists of three lines denoted by H, R, and S corresponding to a Hopf transition, resonance line, and stationary line, respectively. As in Fig. 2, the line S corresponds to a transition with real eigenvalue, while H and R correspond to a transition with purely imaginary eigenvalue at threshold. However, the phase on the right hand side of S is not stationary, since nonzero ϵ_2 does not allow for fixed point solutions. We will term this phase the asymmetric phase, since the limit cycles found typically in this region are asymmetric with respect to the $\dot{x}=x=0$ point. Note, that ϵ_1 and ϵ_2 are no longer small compared to a and b, and therefore the stability region of the conductive phase in Fig. 3 is not in the domain of validity of the analysis presented in Sec. III A and shown in Fig. 2. The case of binary mixture corresponds to $f_1<0$ in Eq. (3.13), which implies that the transition along S to the asymmetric phase is first order. Therefore one finds locally stable asymmetric trajectories also to the left of line S. As one moves away from the line S to the left, one finds that the asymmetric trajectories seem to disappear along the line W, where they either become chaotic (see Fig. 3) or their region of stability shrinks to zero. So, for example, the asymmetric limit cycle for $a=-0.24$ and $b=0.02$ becomes weakly chaotic for $a=-0.24$ and $b=0$. To the left of the line W one still finds periodic and chaotic trajectories. These trajectories disappear along the line C. To the left of this line the only stable solution is the conductive one, namely $x=0$ phase.

We consider the resonance line R and describe the trajectories in the vicinity of this line. At the tip of the tongue ($a=-0.23$, $b=-0.01$) the transition is second order to a symmetric limit cycle with locked frequency $\Omega=\omega/2$. Since Eq. (3.13) contains only odd powers of x, the power spectrum of the time signal of the locked cycle exhibits only the odd harmonics of Ω, i.e., $(2n+1)\Omega$. Above the point A in Fig. 3 the transition is first order, and again to a symmetric limit cycle and locked frequency. Around the point $a=-0.148$ and $b=-0.039$ (denoted by B in Fig. 3) this cycle bifurcates into two coexisting slightly asymmetric limit cycles with more complicated harmonic content. In addition to the locked frequency $\Omega=\omega/2$ and its odd harmonics $(2n+1)\Omega$, one also finds even harmonics at frequencies $2n\Omega$. Moving up along the edge of the resonance tongue one finds that both cycles undergo a cascade of period doublings and result in weakly chaotic orbits at $a=-0.09$, $b=-0.043$. For smaller values of $|a|$ the regions of attraction of these two orbits merge and the resulting orbit has a fully chaotic power spectrum and Lyapunov exponent equal to 0.40 ± 0.02 for $a=-0.07$, $b=-0.043$. For values of a between -0.08 and zero there is chaos on the edge of the resonance tongue. The transition between the conductive and chaotic state is intermittent and does not show hysteresis (as in the case of bimodal maps).[25] In Fig. 4 a typical intermittent trajectory in this region is shown. Note that this intermittent transition is a *direct* transition between the conductive and chaotic state. Going from the tip of the tongue to the right along the edge the transition to the locked state is second order all the way up to a chaotic region denoted by heavy shading in Fig. 3. The chaotic trajectories in this region have their origin in the merging of the basins of attraction of two orbits from the asymmetric phase.

Between the left edge of the resonance tongue and the C line there is a region of coexistence of the conductive and chaotic state. The region of chaotic trajectories extends for negative as well as positive values of a (see Fig. 3). The transition to chaos from the side of the negative values of a is mainly through a period doubling cascade, while from the side of the positive values of a mainly through intermittency. For large positive values of a the limit cycles are usually symmetric. For smaller values of a they undergo a transition (mainly through a chaotic state) to a pair of coexisting asymmetric limit cycles along time T. These asymmetric limit cycles in turn become chaotic via an intermittent transition along the upper boundary of the chaotic region (the heavily shaded region in Fig. 3).

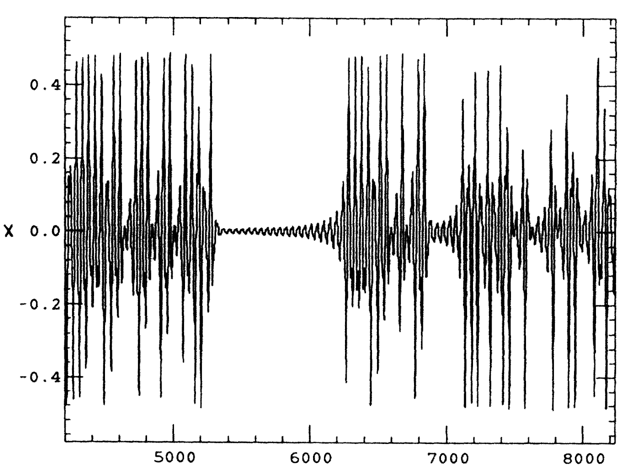

FIG. 4. Intermittent trajectory associated with the transition between the conductive and chaotic state. The solution of Eq. (2.13) is shown as a function of time for $a=-0.05$, $b=-0.045$, $f_1=1$, $f_2=-1$, $f_3=-7$, $\epsilon_1=0.09$, $\epsilon_2=0.08$, $\omega=0.273$, and $\phi=0$.

We have analyzed the phase diagram of Eq. (3.13) for values of ϵ_1, ϵ_2, ω, and ϕ corresponding to a binary mixture (for example the ethanol-water mixture) at room temperature. We choose the following values for the modulation parameters: $\epsilon_1=0.25$, $\epsilon_2=0.14$, $\omega=0.395$, and $\phi=26.6°$, which correspond to the Lewis number $\mathscr{L}=0.02$ and the separation ratio $\Psi=-0.5\times10^{-3}$. The numerical analysis in this case gives results which are qualitatively similar to those shown in Fig. 3. In particular one also finds chaotic trajectories for negative values of a and the intermittent transition between the conductive and chaotic state at the edge of the resonance tongue. In general the chaotic region for negative values of a can be found in cases where ϵ_1 and ϵ_2 are larger than or comparable to a and b as long as the phase ϕ does not approach 90°. If these conditions are not met the chaotic region shrinks and one finds small chaotic regions mainly located in the positive values of a.

IV. CONCLUSIONS

We have analyzed the phase diagram of externally modulated Rayleigh-Bénard system of binary mixtures near the CT point. Numerical integration of the equations of motion shows that in a large part of the physically relevant parameter space this system exhibits chaotic trajectories. The results of the numerical integration for a given choice of the parameters is summarized in Fig. 3. In particular, in some region of the phase diagram chaotic trajectories coexist with the convective phase. Furthermore we show, that the transition between the chaotic and conductive phase is intermittent.

APPENDIX

In the unmodulated case, the phase diagram (see Fig. 1) exhibits a line I_n along which one finds heteroclinic orbit. In the unmodulated case one expects a region in the a-b plane in which such orbits exist. In this appendix we employ the method of Melnikov, in order to calculate the boundaries of this region, for $\epsilon_1\neq0$ and $\epsilon_2=0$. This method enables one to study the stability of planar homoclinic (or heteroclinic) orbits under small perturbation. For further details we refer to Ref. 14, Chap. 4. In order to study the stability of the heteroclinic orbit occurring at I_n under small perturbation due to nonzero $\Delta_1=\epsilon_1/a$ we set $\epsilon_2=0$ in Eq. (2.1) and rescale it as follows:

$$\begin{aligned}&x=\epsilon u,\ \dot{x}=\epsilon^2 v,\ b=-\epsilon^2\nu_1,\ a=\epsilon^2\nu_2\ ,\\&\epsilon_1=\epsilon^2\tilde{\epsilon}_1,\ \Delta_1=\epsilon_1/a=\tilde{\epsilon}_1/\nu_2\ ,\\&\omega\to\epsilon^{-1}\omega,\ \ t\to\epsilon t\ .\end{aligned}\tag{A1}$$

One obtains the following equations:

$$\begin{aligned}&\dot{u}=v\ ,\\&\dot{v}=-\nu_1 u+f_1u^3+\epsilon\{\nu_2 v[1+\Delta_1\cos(\omega t)]-f_2u^2v\}\ .\end{aligned}\tag{A2}$$

To the zeroth order in ϵ Eq. (A2) describes a Hamiltonian system with the Hamiltonian

$$\mathscr{H}(u,v)=\tfrac{1}{2}\nu_1u^2+\tfrac{1}{2}v^2-\tfrac{1}{4}f_1u^4\ .\tag{A3}$$

The phase portrait of this Hamiltonian contains a heteroclinic orbit with energy $\nu_1^2/4f_1$ belonging to the heteroclinic points

$$(u,v)=(\pm\sqrt{\nu_1/f_1},0) . \tag{A4}$$

The parameterization of this orbit is given by

$$\begin{aligned} u_{\pm}^0 &= \pm\sqrt{\nu_1/f_1}\tanh\left[\frac{\nu_1}{2}\right]^{1/2} t , \\ v_{\pm}^0(t) &= \pm\frac{\nu_1}{\sqrt{2}f_1}\left\{\cosh\left[\left[\frac{\nu_1}{2}\right]^{1/2} t\right]\right\}^{-2} . \end{aligned} \tag{A5}$$

We calculate the Melnikov function $\mathcal{M}(\nu_1,\nu_2,\Delta_1,\omega,t_0)$ (see Ref. 14, p. 191) belonging to u_+^0 and v_+^0 (the calculation for u_-^0 and v_-^0 is identical). This function is given by

$$\mathcal{M}(\nu_1,\nu_2,\Delta_1,\omega,t_0)=\int_{-\infty}^{+\infty} dt(v_+^0)^2(\nu_2\{1+\Delta_1\cos[\omega(t+t_0)]\}+f_2(u_+^0)^2) , \tag{A6}$$

where $t\in[0,2\pi/\omega]$. In the absence of modulation the Melnikov function is time independent and can be evaluated directly, yielding

$$\int_{-\infty}^{+\infty} dt(v_+^0)^2[\nu_2-f_2(u_+^0)^2]=\frac{2}{3}\frac{\nu_1^3}{f_1}\left[\frac{2}{\nu_1}\right]^{1/2}\left[\frac{\nu_2}{\nu_1}+\frac{1}{5}\frac{f_2}{f_1}\right] . \tag{A7}$$

A zero of $\mathcal{M}(\nu_1,\nu_2,\Delta_1,\omega,t_0)$ determines a line in parameter space along which a heteroclinic orbit occurs. From Eq. (A7) we obtain $a/b=f_2/5f_1$ for this heteroclinic orbit. This result for the line I_n was obtained previously by various authors.[6,14]

The integral containing $\cos[\omega(t+t_0)]$ can be evaluated by the method of residues yielding:

$$\nu_2\Delta_1\int_{-\infty}^{+\infty} dt(v_+^0)^2\cos[\omega(t+t_0)]=\frac{\Delta_1\nu_1\nu_2}{2f_1}\pi\omega\left[\frac{\omega^2\nu_1}{12}+\frac{2}{5}\right]\cos(\omega t_0)\left[\sinh\left[\frac{\omega}{\sqrt{2\nu_1}}\pi\right]\right]^{-1} . \tag{A8}$$

The final result for the time dependent Melnikov function $\mathcal{M}(\nu_1,\nu_2,\Delta_1,\omega,t_0)$ is obtained by combining the results given in (A7) and (A8). The occurrence of heteroclinic orbits is determined by zeros of $\mathcal{M}(\nu_1,\nu_2,\Delta_1,\omega,t_0)$. Simple zeros indicate an occurrence of a transversal heteroclinic orbit and double zeros indicate the occurrence of quadratic heteroclinic tangencies. For $t_0\in[0,2\pi/\omega]$ one finds double zeros for $t_0=0$ and π/ω and simple zeros for intermediate values of t_0. The region in the a-b plane in which heteroclinic orbits exist is therefore bounded by the two lines I_n^1 defined by $\mathcal{M}(\nu_1,\nu_2,\Delta_1,\omega,t_0=0)=0$ and I_n^2 defined by $\mathcal{M}(\nu_1,\nu_2,\Delta_1,\omega,t_0=\pi/\omega)=0$

ACKNOWLEDGMENTS

This work was supported by the U.S.-Israel Binational Science Foundation, by the Bat Sheva de-Rothschild Fund for Advancement of Science and Technology, and by the Israel Academy of Sciences and Humanities, Basic Research Foundation. One of us (V.S.) acknowledges the support of the M. M. Boukstein Foundation.

[1]F. H. Busse, Rep. Prog. Phys. **41**, 1929 (1978).
[2]L. A. Segel, J. Fluid Mech. **38**, 203 (1969); A. C. Newell and J. A. Whitehead, *ibid.* **38**, 279 (1969).
[3]P. Berge and M. Dubois, Contemp. Phys. **25**, 535 (1984).
[4]H. Brand and V. Steinberg, Phys. Lett. **93A**, 333 (1983).
[5](a) V. Steinberg, J. Appl. Math. Mech. (USSR) **35**, 335 (1971); (b) D. T. J. Hurle and F. Jakeman, J. Fluid Mech. **47**, 667 (1971); (c) R. S. Schechter, M. J. Velarde, and J. K. Platten, Adv. Chem. Phys. **26**, 265 (1974).
[6]H. Brand, P. C. Hohenberg, and V. Steinberg, Phys. Rev. A **27**, 591 (1983); **30**, 2548 (1984).
[7]P. H. Coullet and E. A. Spiegel, SIAM. J. Appl. Math. **43**, 776 (1983).
[8]E. Knobloch and M. R. B. Proctor, J. Fluid Mech. **108**, 291 (1981).
[9]E. Knobloch and J. Guckenheimer, Phys. Rev. A **27**, 408 (1983).
[10]B. J. A. Zielinska, D. Mukamel, F. Steinberg, and S. Fishman, Phys. Rev. A **32**, 702 (1985).
[11]H. Brand and V. Steinberg, Physica **119A**, 327 (1983).
[12]M. West, and V. S. Arpaci, J. Fluid Mech. **36**, 613 (1969).
[13]B. J. A. Zielinska, D. Mukamel, and V. Steinberg, Phys. Rev. A **33**, 1454 (1986).
[14]J. Guckenheimer and P. Holmes, *Nonlinear Oscillations, Dynamical Systems and Bifurcations of Vector Fields* (Springer, New York, 1983), Chaps. 3 and 7.
[15]G. Ahlers, P. Hohenberg, and M. Lucke, Phys. Rev. Lett. **53**, 48 (1984).
[16]G. Ahlers, P. Hohenberg, and M. Lucke, Phys. Rev. A **32**, 3493 (1985); **32**, 3519 (1985).
[17]C. W. Meyer, G. Ahlers, and D. S. Cannell, Bull. Am. Phys. Soc. **31**, 473 (1986).
[18]J. K. Bhattacharjee and K. Banerjee, Phys. Rev. B **30**, 1336 (1984).
[19]A. Agarwal, J. K. Bhattacharjee, and K. Banerjee, Phys. Rev. B **30**, 6458 (1984).

[20]Note that when higher-order terms are added to Eq. (2.1) the line I_n exhibits hysteretic behavior between the limit cycle and the stable fixed points.

[21]M. W. Hirsch and S. Smale, *Differential Equations, Dynamical Systems and Linear Algebra* (Academic, New York, 1974).

[22](a) I. Rehberg and G. Ahlers, Phys. Rev. Lett. **55**, 500 (1985); (b) G. Ahlers and I. Rehberg, *ibid.* **56**, 1373 (1986); (c) U. Gao and R. P. Behringer, Phys. Rev. A **34**, 697 (1986).

[23](a) R. W. Walden, P. Kolodner, A. Passner, and C. M. Surko, Phys. Rev. Lett. **55**, 496 (1985); (b) E. Moses and V. Steinberg, Phys. Rev. A **34**, 693 (1986).

[24]V. Steinberg and H. Brand, Phys. Rev. A **30**, 3366 (1984).

[25]C. Tresser, P. Coullet, and A. Arneodo, J. Phys. Lett. **41**, L243 (1980).